

Enabling Fast-Charging and High Specific Capacity of Li-Ion Batteries with Nitrogen-Doped Bilayer Graphdiyne: A First-Principles Study

Minh Tam Le,^[a] Liang-Yin Kuo,^{*[b, c, d]} Yi-Zhan Wu,^[b] Martin Ihrig,^[e] and Nguyet N. T. Pham^{*[a, f]}

Carbon-based materials are the most important anode materials for Li-ion batteries (LIBs). To improve the electrochemical performance of LIBs for high energy density and fast charging, advanced carbon allotropes are in the research focus. In this work, we applied the density functional theory to investigate the atomic and electronic structures as well as high Li-ion specific capacity of graphdiyne (GDY). The atomic structures of monolayer graphdiyne (MGDY), bilayer AB(β_1)-stacking graphdiyne (AB(β_1)BGDY) and nitrogen-doped AB(β_1)BGDY (N-AB(β_1)BGDY) at different lithiation states were thoroughly investigated. The AB(β_1)BGDY and N-AB(β_1)BGDY exhibit promising

characteristics in Li-ion adsorption and intercalation, enhancing its specific capacity from 744 mAhg⁻¹ in the monolayer GDY to 807 mAhg⁻¹ in the bilayer. Besides increasing the capacity through a bilayer-structure, it is possible to tailor its structural stability and band gap by doping. Especially shown for N-AB(β_1)BGDY (~1%), an increased structural stability and a decreased band gap of 0.24 eV is found. While this means that N doping in AB(β_1)BGDY can lead to longer-lasting and more stable operable high-capacity anodes in LIBs, it increases the open-circuit voltage (OCV).

Introduction

Advanced energy storage technology is relevant to the progress and further develop electronic devices,^[1] battery electric vehicles,^[2] and the smart grid.^[3] Hydrogen storage media^[4], supercapacitors,^[5] rechargeable batteries,^[6] and other innovative energy storage technologies are a few examples of those that have attracted a lot of academic and industrial interest. Among rechargeable batteries, Lithium-ion batteries (LIBs) are most prominent and are extensively employed in various portable devices such as cellular phones, laptops, and wearable

devices.^[7] Beyond these applications, LIBs are the candidate of choice for integration into (hybrid) electric vehicles.^[8]

Further advances in LIBs are related to advances in the utilized (electrode) materials. Predominantly the anode material requires improvement. The anode is commonly a graphite-based material with a theoretical capacity of 372 mAhg⁻¹.^[8] Carbon-based materials have become the dominant anode for LIBs because of their special structure with sp^2 - and sp^3 -C hybridization, resulting in high electronegativity and porous density. They are beneficial for Li-ion adsorption and diffusion.^[9] Moreover, carbon allotropes have high chemical, thermal and electrochemical stability, reversible Li-ion storage, and more safety than metallic Li anodes.^[10] Graphite has a structure based on 6 C atoms in which 1 Li-ion can be stored, resulting in a composite of LiC₆ at 0.1 V~0.2 V vs Li/Li⁺.^[8] The sp^2 -bonded carbon of graphite improves Li-ion intercalation.^[8,11] However, graphite-based anodes have limited capacity and determine the fast-charge capability of the entire LIB. While the capacity aspects could be covered by metallic Li anodes (3860 mAhg⁻¹^[12]) safety concerns due to Li dendrite formation remain.^[13] Another alternative would be Si-based anodes. Si-based anodes have an even higher capacity (4200 mAhg⁻¹^[14]) than metallic Li anodes but due to the high swelling during cycling leads to rapid degradation and ultimately to a failing LIB.^[14] Thus, carbon-based anodes are still the most used anodes in LIBs and improvements in carbon-based materials could elevate the performance of LIBs. In addition, a graphite-based anode material might be applicable in current LIB technology even on industrial scale. Therefore, various carbon-based anode materials including inorganic electrode materials such as carbon nitride (2092 mAhg⁻¹^[15]), graphene (744 mAhg⁻¹^[16]), carbon nanotubes (1000 mAhg⁻¹^[17]), and graphyne (558 mAhg⁻¹^[18]) as well as organic materials like covalent organic frameworks

[a] M. Tam Le, N. N. T. Pham
Faculty of Chemistry, University of Science, 227 Nguyen Van Cu, Ho Chi Minh City 700000, Viet Nam
E-mail: ptntnguyet@hcmus.edu.vn

[b] L.-Y. Kuo, Y.-Z. Wu
Department of Chemical Engineering, Ming Chi University of Technology, No.84, Gungjuan Rd., Taishan Dist., New Taipei City 243303, Taiwan
E-mail: lkuo@mail.mcut.edu.tw

[c] L.-Y. Kuo
Center for Sustainability and Energy Technologies, Chang Gung University, No.259, Wenhua 1st Rd., Guishan Dist., Taoyuan City 33302, Taiwan

[d] L.-Y. Kuo
Sustainable Electrochemical Energy Development Center, National Taiwan University of Science and Technology, No.43, Keelung Rd., Sec.4, Da'an Dist., Taipei City 106335, Taiwan

[e] M. Ihrig
Department of Chemical Engineering, National Taiwan University of Science and Technology, No.43, Keelung Rd., Sec.4, Da'an Dist., Taipei City 106335, Taiwan

[f] N. N. T. Pham
Faculty of Chemistry, University of Science, Vietnam National University, 227 Nguyen Van Cu, Ho Chi Minh City 700000, Viet Nam

Supporting information for this article is available on the WWW under <https://doi.org/10.1002/batt.202400352>

(COFs)^[19] and covalent triazine framework (CTF-1)^[20] are popular choices that could increase the capacity of current LIBs.^[21] The inorganic materials, in particular, exhibit relatively high electronic conductivity, contributing to their tremendous success in both applications and research. Among those, graphdiyne (GDY) has gained much attention because of its two topological acetylenic links ($-C=C-C=C-$) including sp - and sp^2 -C hybridization.^[22] The $sp-sp^2$ planar GDY structures stack together through van der Waals forces and $\pi-\pi$ interaction, leading to uniformly dispersed pore configuration and tunable electronic structure properties.^[22c] Furthermore, the layered GDY structure exhibits curvature, which is similar to graphene and can maintain structural stability during de-/lithiation. Sun et al.^[18] reported that monolayer GDY (MGDY) can support a maximum Li-ion capacity of 744 mAh g^{-1} with $Li_{24}C_{72}$ composition by density functional theory (DFT) calculation. They suggested that extending the acetylenic chain supports the increase of the capacity for Li-ion storage due to higher internal structural stability through the acetylenic chain. Zhang et al.,^[23] however studied Li-ion storage properties of bilayer GDY (BGDY) in order to understand the volume expansion on multilayer anode for LIBs using DFT. Their results indicate that the interlayer distance of BGDY has influences on its capacity and conductivity properties.^[22c] In our previous work, we simulated the atomic and electronic structures of BGDY. The simulated interlayer distance of BGDY is found to be 3.400~3.420 Å,^[22c] which is larger than that of graphite (3.350 Å).^[24] The increased distance of BGDY improves Li-ion adsorption and diffusion.

Doping heteroatomic atoms into BGDY like boron (B) and nitrogen (N) atoms which exhibit higher electronegativity than carbon (C), is one of the most beneficial strategies to improve electrochemical performances.^[25] With N (0.650 Å) possessing a similar radius to C (0.700 Å) and a greater electronegativity than both C and B, it proves to be particularly effective in altering the electronic properties of carbon-based materials. This includes enhancements in electron affinity and conductivity. Thus N is expected to exhibit greater compatibility with Li-ions than B, making it a focus of extensive research into the effects of N doping on carbon-based materials. Different N-doped positions such as sp -N, sp^2 -N (graphitic N and pyridinic N) and amino-N have been discussed for GDY structure.^[22c,26] The sp -N and sp^2 -N doping have been found to increase the capacity of GDY.^[27] Moreover, Liu et al.^[28] indicated that the sp -N site is the most favorable position for N doping in GDY. We have studied the structural stability of BGDY with N doping by DFT. The results indicate that N-doped BGDY where N replaces C in the sp -C site has the lowest cohesive energy indicative of the most favorable N-doped BGDY structure.^[22c] In this work, we studied the atomic structures of MGDY, BGDY and N-doped BGDY with various states of Li-ion intercalation to understand the effect of N doping on the capacity of Li-ion storage in BGDY by DFT calculations. We calculated the maximum Li-ion storage capacity of BGDY before and after N doping. A detailed discussion of interlayer distance, Li-ion adsorption energy, voltage among MGDY, BGDY, and N-doped BGDY is provided in this work.

Methodology

Spin-polarized density functional theory (DFT) calculations were performed using the generalized gradient approximation (GGA)^[29] implemented in the Vienna Ab Initio Simulation Package (VASP).^[30] The Perdew-Burke-Ernzerhof (PBE)^[29] functional was employed in GGA to describe the exchange-correlation energy, which has been well-studied for carbon-based systems in previous works.^[22c,31] DFT with Grimme's D3 (DFT-D3)^[32] method was utilized to correct van der Waals (vdW) interactions for monolayer GDY (MGDY) and bilayer GDY (BGDY). The Atomistic structure of MGDY and BGDY were optimized by a 2×2 supercells with a vacuum of 22 Å along z-direction. Thus, we have 72 C atoms and 144 C atoms for MGDY and BGDY, respectively. However, N-doped BGDY where 1 N replaces 1 C in sp -N site has 143 C atoms and 1 N atom. The maximum number of Li-ion storage was determined by DFT-PBE calculation. A Monkhorst-Pack k -points of $1\times 1\times 1$ was employed for geometry optimizations, while a $3\times 3\times 1$ k -points mesh was utilized for electronic structure calculations. The energy and force convergence criteria is 10⁻⁵ eV and 0.02 eVÅ⁻¹, respectively.

Results and Discussion

The optimized structures of monolayer GDY (MGDY), bilayer GDY (BGDY), and BGDY with nitrogen doping (N-BGDY) were described in our previous work using DFT.^[22c] In Figure 1, we illustrate the top and side views of the most energetically favorable structures of MGDY, AB(β_1)BGDY and N-AB(β_1)BGDY in a $2\times 2\times 1$ supercell. The figure shows triangular pores surrounded by benzene rings and butadiyne bonds, namely 6 C and 18 C hexagons for each structure. Through DFT analysis, the uniformly distributed pores exhibit an average diameter of ~5.42 Å. Furthermore, the results reveal that BGDY with Bernal AB of carbon stacking mode in bilayer graphene, namely AB(β_1)BGDY represents the most favorable structure, which is consistent with the experimental work^[33] (Figure 1b). Moreover, the most energetically favorable N doping site (sp -N) on our BGDY, referred to as AB(β_1)BGDY configuration (~1% N doping) is illustrated in Figure 1c.

The lattice parameters a and b of MGDY are calculated as ~18.94 Å with four distinct types of C–C bonds described as c1 (sp^2 carbon), c2 (sp^2-sp carbon), c3 (triple sp carbon) and c4

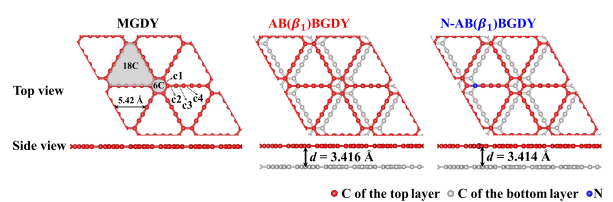


Figure 1. Top and side views of the most favorable structure of (a) MGDY (b) AB(β_1)BGDY and (c) N-AB(β_1)BGDY including their interlayer distance (d). The benzene ring is labeled with 6 C. The diameter of the triangular pores (labeled as 18 C) is 5.42 Å. c1, c2, c3, and c4 represents sp^2 carbon, sp^2-sp carbon, triple sp carbon and single sp carbon, respectively.

(single *sp* carbon). The average bond length for c1, c2, c3, and c4 in MGDY are found to be 1.429 Å, 1.404 Å, 1.226 Å, and 1.344 Å, respectively, consistent with the results reported by previous work.^[22c,33–34] Moreover, our analysis indicates that AB(β_1)BGDY and N-AB(β_1)BGDY exhibit similar bond length of MGDY. Table 1 provides a detailed analysis of bond lengths. The interlayer distance (d) of AB(β_1)BGDY and N-AB(β_1)BGDY shows minimal variation with values of 3.416 Å and 3.414 Å, respectively. This suggests that a minor N doping (~1%) does not alter the AB(β_1)BGDY configuration. N-AB(β_1)BGDY used in an LIB as anode materials might therefore show higher cycling stability and could lead to longer cycling while retaining its initial capacity than AB(β_1)BGDY.

The band structures reveals a reduction in the band gap, showing the value of 0.55 eV (MGDY), 0.43 eV (AB(β_1)BGDY) and 0.24 eV (N-AB(β_1)BGDY). Notably, N-AB(β_1)BGDY exhibits the smallest band gap, which agrees with our previous findings for a comparable structure (0.16 eV) and indicates its superior electronic conductivity (Figures 2a–c).^[22c] N-AB(β_1)BGDY also shows a narrower band gap compared to other stacking modes (e.g., AB(β_2)) in BGDY with N doping.^[22c] This suggests that the number of layers and stacking mode can influence the electronic structures and thus the electronic properties of GDY. Moreover, N-doping causes a shift of the Fermi energy (dash line) to higher energy level. This shift leads to the conduction band intersecting the Fermi energy, thereby facilitating charge transfer of N-AB(β_1)BGDY. This behavior is also evidenced in the charge density difference (CDD) analysis for N-AB(β_1)BGDY, where partial yellow and blue features on C and N are observed (Figure 2d). In particular, the large blue features on N show that the valence electrons of N participate in the conjugation system within the carbon chain and lose charge on the N atom. This implies that N doping into AB(β_1)BGDY increases the conju-

gated charge density and enhances its electronegativity. Therefore, N doping of AB(β_1)BGDY might enhance the de-/lithiation process, allowing for higher C-rates in a LIB anode.

Afterwards a detailed investigation of the Li-ion storage capacity within MGDY, AB(β_1)BGDY and N-AB(β_1)BGDY was conducted. The Li-ion adsorption site was determined via the DFT. The average adsorption energy (E_{av-ads}) for all Li-ions follows by eq (1):^[18,23]

$$E_{av-ads} = \frac{E_{GDY} - E_{nLi+GDY} + nE_{Li}}{n} \quad (1)$$

where E_{GDY} , $E_{nLi+GDY}$, and E_{Li} is the total energy of monolayer/bilayer GDY, the monolayer/bilayer GDY with total number of n absorbed Li-ions, and a single Li in vacuum space, respectively.

To determine the most favorable Li-ion adsorption site on GDY structures, we simulated 1 Li-ion adsorbed into the hole (H0) and below the hole at different distances ($h_1 = 1$ Å and $h_2 = 2$ Å) from the surface of 6 C and 18 C hexagons in MGDY. The positions of H0, h_1 , and h_2 before and after the geometry optimization are illustrated in Figure S1. In all three cases, the 1 Li-ion consistently shift ~1.707 Å below the hole for the 6 C hexagon, while it is located within the hole (H0) for the 18 C hexagon (Figures 3a–b). The E_{ads} of 1 Li-ion is 1.97 eV and 2.74 eV for the 6 C hexagon and the 18 C hexagon, respectively. This indicates that 1 Li-ion prefers to occupy the 18 C hexagon due to the weaker electrostatic interaction between the carbon rings and the Li-ion. Furthermore, we simulated 3 Li-ions within the hole (H0) and at various distances for the 18 C hexagon (Figure S1). Our results reveal a slight deviation in distance (~0.964 Å) from the surface for three Li-ions within the 18 C hexagon (i.e., h_1 position at 1 Å). Within this scenario the highest calculated E_{ads} is 2.11 eV (Figure 3c). However, the E_{ads} difference at H0 and h_1 is relatively small (~0.09 eV). In the following, we will explore the maximum Li-ion storage, their interactions with carbon atoms, as well as the theoretical capacity and open-circuit voltage during lithiation and delithiation.

To predict the maximum Li-ion storage, additional Li-ions adsorbed on MGDY, AB(β_1)BGDY and N-AB(β_1)BGDY were considered. The maximum number of Li-ions was determined based on structural stability after geometry optimization. Our results show a gradual increase in Li-ion storage capacity on MGDY, reaching a maximum at 24 Li-ions. Figure 4a displays the configurations of MGDY during lithiation from label iii to v,

Table 1. Average bond lengths of MGDY, AB(β_1)BGDY, and N-AB(β_1)BGDY across c1 (*sp*² carbon), c2 (*sp*²-*sp* carbon), c3 (triple *sp* carbon) and c4 (single *sp* carbon), as well as N–C bond lengths for N-AB(β_1)BGDY (see also Figure 1).

Anode materials	Carbon bonds (Å)				N–C bonds (Å)	
	c1	c2	c3	c4	N–C _{sp²}	N–C _{sp}
MGDY	1.429	1.404	1.226	1.344	-	-
AB(β_1)BGDY	1.429	1.401	1.228	1.341	-	-
N-AB(β_1)BGDY	1.428	1.402	1.227	1.341	1.355	1.197

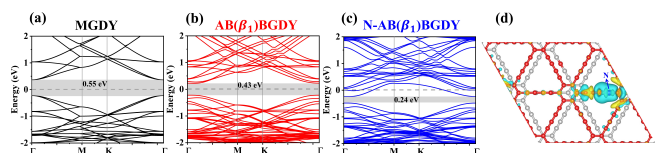


Figure 2. The band structures of (a) MGDY (b) AB(β_1)BGDY and (c) N-AB(β_1)BGDY and (d) charge density difference (CDD) for N-AB(β_1)BGDY. The yellow and blue feature represents charge gain and loss, respectively. The isosurface value of 0.0015 e/Å³. The band gap is depicted for each structure.

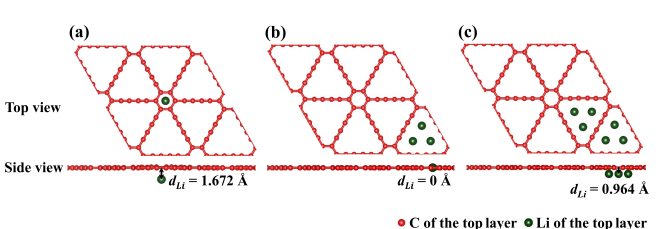


Figure 3. The top and side views of the most favorable structure of one Li-ion (a) above the hole ($d_{Li} = 1.707$ Å) for 6 C hexagon (b) within the hole ($d_{Li} = 0$ Å) for 18 C hexagon and (c) three Li-ions below the hole ($d_{Li} = 0.964$ Å) for 18 C hexagon in MGDY.

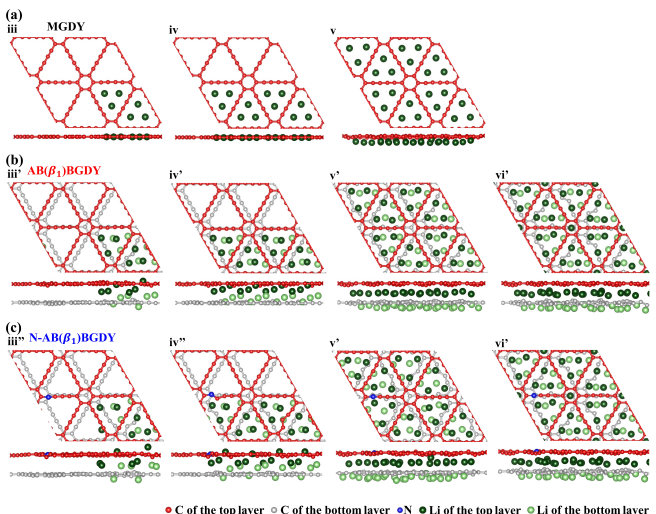


Figure 4. Geometries at various lithiation states of (a) MGDY, (b) AB(β_1)BGDY and (c) N-AB(β_1)BGDY.

while labels i and ii corresponding to MGDY configurations with 1 and 3 Li-ions are shown in Figure 3b and Figure S2. Notably, when the number of Li-ions reaches 24 (label v), there is a small migration of Li-ions away from the surface which is similar to Figure 3c due to the repulsion between carbon rings and Li-ions. However, the MGDY structure maintains its integrity, suggesting high stability during cycling. With further lithiation and an increase in Li-ion number to 28 or 32 Li-ions, significant distortions and deformations in the carbon rings become evident, indicating the instability of MGDY under these conditions (Figure S2). Thus, MGDY is possible to accommodate 1 to 24 Li-ions, indicating the formation of a LiC₃ (Li₂₄C₇₂) composite. Whereas AB(β_1)BGDY which comprises two layers of MGDY exhibits the maximum Li-ion storage capacity of 1 to 52 (label i' to vi'), leading to the formation of a LiC_{2.77} (Li₅₂C₁₄₄) composite. During the initial stage of lithiation (label i' and ii' in Figure S3a), we simulated the adsorption of 1 Li-ion and 3 Li-ions in each layer into the 18 C hexagon hole of AB(β_1)BGDY. The results show that Li-ions spontaneously migrate away from the surface of AB(β_1)BGDY after geometry optimization, indicating that bilayer GDY undergoes both interlayer insertion/extraction and surface absorption/desorption. With further lithiation to accommodate 6 and 12 Li-ions (label iii' and iv') within the 18 C hexagon hole on each surface layer (12 and 24 Li-ions in total), the migration of Li-ions becomes more significant, with a greater number of Li-ions intercalating into the AB(β_1)BGDY layer. The migration of Li-ions can be attributed to the repulsion between carbon rings and Li-ions, while an attractive interaction occurs among Li-ions. This behavior has been previously reported by Juarez et al.^[35] using the DFT method. They suggest that a lattice of carbon atoms induces an apparent attraction between Li-ions. As the number of Li-ions increases to 48 (label v'), a stronger repulsion between carbon rings and Li-ions induces the migration of 24 Li-ions away from the surface of AB(β_1)BGDY. However, another 24 Li-ions are located below the second layer of AB(β_1)BGDY, showing a

smaller deviation from the surface, which is similar to the behavior simulated in MGDY. When further Li-ions are added (52 Li-ions in total), the additional Li-ions intercalate into the interlayer space and are allowed to store within the AB(β_1)BGDY structure (label vi'). As shown in Figure 4b, 4 additional Li-ions can be positioned below the benzene rings (6 C). However, this intercalation leads to an increase in d value to 3.491 Å and thus a distortion of the triangular pores and carbon rings. The volume expansion for AB(β_1)BGDY in the composition of LiC_{2.77} is calculated to be 2.27%. While a slight distortion appears beneficial to increase the Li-ion storage, an excess of Li-ions will lead to a structural collapse of AB(β_1)BGDY. As calculated, storing 56 Li-ions within AB(β_1)BGDY leads to severe distortion of the triangular pores and the carbon rings resulting in a thermodynamically unstable structure during cycling (Figure S4). N-AB(β_1)BGDY contributes an equal amount of Li-ions storage as AB(β_1)BGDY, with 1 to a maximum of 52 Li-ions (LiC_{2.77}) as shown in Figure S3b (label i''' and ii''') and Figure 4c (label iii''' to vi''''). This indicates that the mechanism of Li-ions storage in BGDY involves a combination of Li-ions intercalating into the interlayer space and absorbing onto the surfaces. Although N-AB(β_1)BGDY has the same Li-ions storage capacity as AB(β_1)BGDY, it exhibits a reduced volume expansion of 0.33% ($d=3.48$ Å for vi''') compared to AB(β_1)BGDY. Therefore, N-AB(β_1)BGDY exhibits greater stability than AB(β_1)BGDY during de-/lithiation, suggesting enhanced cyclability. The atomic structures at various lithiation states are supported by the calculation of the $E_{\text{av-ads}}$ values for MGDY, AB(β_1)BGDY and N-AB(β_1)BGDY during lithiation in Figure S5. These values ($E_{\text{av-ads}}$) are higher than the experimental or theoretical bulk Li cohesive energy (1.600–1.670 eV^[13,23,36]) which avoid the formation of Li cluster.

The theoretical capacity (C_p) and open-circuit voltage (OCV) of MGDY, AB(β_1)BGDY and N-AB(β_1)BGDY are calculated by eq (2)^[37] and eq (3)^[23] as shown below:

$$C_p = \frac{nF}{3600M_{\text{GDY}}} \quad (2)$$

$$\text{OCV} = \frac{E_{\text{GDY}} - E_{n\text{Li+GDY}} + E_{\text{Li-bulk}}}{ne} \quad (3)$$

where F is the Faraday constant (taken as 96500 mAh), and M_{GDY} is the mass of the molecular weight of monolayer/bilayer GDY. $E_{\text{Li-bulk}}$ is the energy of bulk body-centered cubic (bcc) Li. Based on the calculations described above, MGDY can store up to 24 Li-ions and thus reaches a maximum capacity of 744 mAhg⁻¹ (LiC₃). This value is higher than that of graphyne (558 mAhg⁻¹, LiC₄)^[10a,18,32,38] and graphene (372 mAhg⁻¹, LiC₆).^[16,18] The increased capacity of MGDY is found in the extension of the acetylenic chain that improves the interactions with Li-ions in MGDY. The calculated OCV for MGDY is in the range of 1.10 to 0.25 V (Li_{0.04}C₃ → LiC₃). Thus, the average OCV is 0.68 V for MGDY (Figure 5). In AB(β_1)BGDY and N-AB(β_1)BGDY a maximum of 52 Li-ions is absorbed and results in a maximum capacity of 807 mAhg⁻¹ (LiC_{2.77}). While the Li-ion storage capacity is same for AB(β_1)BGDY and N-AB(β_1)BGDY a difference is found in their

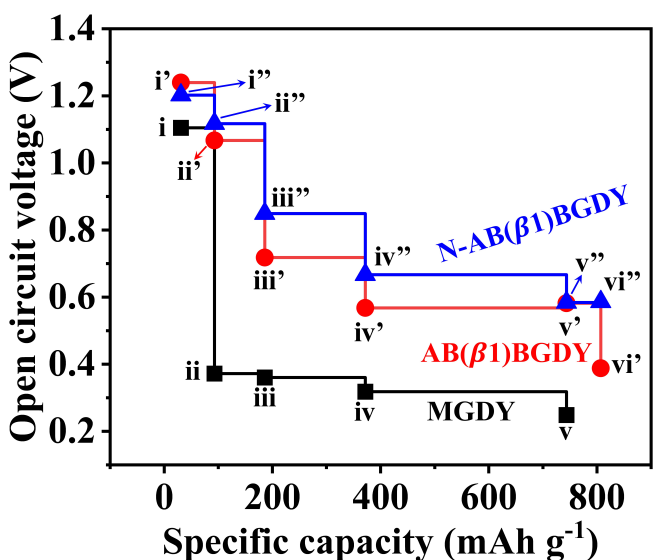


Figure 5. Calculated open-circuit voltage (OCV) and specific capacity of MGDY, AB(β_1)BGDY and N-AB(β_1)BGDY at various lithiation states.

OCV. The calculated OCV of AB(β_1)BGDY is in a range of 1.24~0.39 V ($\text{Li}_{0.04}\text{C}_{2.77} \rightarrow \text{LiC}_{2.77}$) with an average OCV of 0.82 V. However, the N-AB(β_1)BGDY shows 1.20~0.59 ($\text{Li}_{0.04}\text{C}_{2.77} \rightarrow \text{LiC}_{2.77}$) with an average OCV of 0.90 V. Noted that the OCV values are neither close to zero nor negative, further mitigating the risk of Li ion clustering and Li dendrite formation. Therefore, both AB(β_1)BGDY and N-AB(β_1)BGDY have their own advantages. While AB(β_1)BGDY provides a lower OCV and can lead, assembled as an anode material in a full LIB, to a higher energy density, the N-AB(β_1)BGDY has a higher electronic conductivity and possesses superior structural stability which can lead to more stable cycling and higher capacity retention. Through tailoring of the N doping in AB(β_1)BGDY high energy through a larger voltage-window in the LIB with stable cycling is achievable. The presented N-doped-AB(β_1)BGDY is promising due to its elevated capacity in comparison with other carbon-based materials (Table S1).

Conclusions

This work evaluates the possibility of using as attractive anode material in LIBs. For the simulation-based approach monolayer GDY (MGDY), bilayer graphdiyne (BGDY) with AB(β_1 -stacking), and N-doped AB(β_1)BGDY were selected and analyzed. Through the DFT calculations it was found that the maximum Li-ion storage capacity of the materials is: 744 mAh $^{-1}$ (MGDY), 807 mAh $^{-1}$ (AB(β_1)BGDY), and 807 mAh $^{-1}$ (N-doped AB(β_1)BGDY). The elevated specific Li-ion capacity in the bilayer graphdiyne makes it more attractive than the monolayer structure considering the capacity. However, regarding stability during de-/lithiation the MGDY is the material of choice. In order to combine high capacity with stability, N doping of the bilayer AB(β_1)BGDY is possible.

N doping tailors the properties of the bilayer graphdiyne and allows to stabilize the structure, reducing volume expansion by 0.33% compared to AB(β_1)BGDY. Increased electronic conductivity with a small band gap of 0.24 eV facilitates stable de-/lithiation, enabling longer cycling in LIB. However, the increased conductivities come at the expense of an increased OCV (0.90 V instead of 0.82 V) and thus a lower total energy in a LIB when N-doped bilayer graphdiyne is used. In the following studies, the effect of N doping should be addressed in detail as it allows tailoring the properties of bilayer graphdiyne to obtain either a high energy or power LIB or ideally can fulfil both criteria.

Acknowledgements

We gratefully acknowledge financial support from the Ministry of Science and Technology, Taiwan (Project No: NSTC 111-2222-E-131-002), and the Ministry of Education of Taiwan through the Sustainable Electrochemical Energy Development Center (SEED), part of the Featured Areas Research Center Program. We also thank Chang Gung University for their support (URRPD2 N0021). Computing resources were generously provided by the National Center for High-performance Computing (NCHC) on Taiwania 3 in Hsinchu, Taiwan. M. I. thanks the Alexander-von-Humboldt Foundation and the Taiwanese National Science and Technology Council for funding (grant no.: 112-2927-I-011-505). This research is also funded by the University of Science, VNU-HCM under grant number T2023-31.

Conflict of Interests

The authors declare no conflict of interest.

Data Availability Statement

The data that support the findings of this study are available in the supplementary material of this article.

Keywords: Li-ion batteries • Carbon-based anodes • DFT • Graphdiyne

- [1] P. G. Bruce, S. A. Freunberger, L. J. Hardwick, J.-M. Tarascon, *Nat. Mater.* **2012**, *11*, 19–29.
- [2] G. Zheng, S. W. Lee, Z. Liang, H.-W. Lee, K. Yan, H. Yao, H. Wang, W. Li, S. Chu, Y. Cui, *Nat. Nanotechnol.* **2014**, *9*, 618–623.
- [3] F. Cheng, J. Liang, Z. Tao, J. Chen, *Adv. Mater.* **2011**, *23*, 1695–1715.
- [4] R. Liu, Y. Zhao, T. Chu, *Chem. Commun.* **2015**, *51*, 2429–2432.
- [5] Z. Tan, G. Chen, Y. Zhu, *Nanocarbons Adv. Energy Storage* **2015**, *1*, 211–225.
- [6] G. Binitha, A. G. Ashish, D. Ramasubramonian, P. Manikandan, M. M. Shajumon, *Adv. Mater. Interfaces* **2016**, *3*, 1500419.
- [7] K. Feng, W. Ahn, G. Lui, H. W. Park, A. G. Kashkooli, G. Jiang, X. Wang, X. Xiao, Z. Chen, *Nano Energy* **2016**, *19*, 187–197.
- [8] A. Perner, J. Vetter, in *Advances in Battery Technologies for Electric Vehicles*, Elsevier, **2015**, 173–190.
- [9] a) R. Kumar, S. Sahoo, E. Joanni, R. K. Singh, W. K. Tan, K. K. Kar, A. Matsuda, *Prog. Energy Combust. Sci.* **2019**, *75*, 100786; b) E. Wang, M.

- Chen, X. Guo, S. L. Chou, B. Zhong, S. X. Dou, *Small Methods* **2020**, *4*, 1900163.
- [10] a) X. Dou, I. Hasa, D. Saurel, C. Vaalma, L. Wu, D. Buchholz, D. Bresser, S. Komaba, S. Passerini, *Materials Today* **2019**, *23*, 87–104; b) J. Ming, Z. Cao, Y. Wu, W. Wahyudi, W. Wang, X. Guo, L. Cavallo, J.-Y. Hwang, A. Shamim, L.-J. Li, *ACS energy letters* **2019**, *4*, 2613–2622.
- [11] K. Takahashi, V. Srinivasan, *J. Electrochem. Soc.* **2015**, *162*, A635.
- [12] a) W. Xu, J. Wang, F. Ding, X. Chen, E. Nasybulin, Y. Zhang, J.-G. Zhang, *Energy Environ. Sci.* **2014**, *7*, 513–537; b) M. Qi, L. Xie, Q. Han, L. Zhu, L. Chen, X. Cao, *J. Energy Storage* **2022**, *47*, 103641.
- [13] H. J. Hwang, J. Koo, M. Park, N. Park, Y. Kwon, H. Lee, *J. Phys. Chem. C* **2013**, *117*, 6919–6923.
- [14] H. Zhao, J. Li, Q. Zhao, X. Huang, S. Jia, J. Ma, Y. Ren, *Electrochem. Energy Rev.* **2024**, *7*, 11.
- [15] A. Ghosh, S. Mandal, P. Sarkar, *ChemPhysChem* **2022**, *23*, e202200182.
- [16] P. Nzereogu, A. Omah, F. Ezema, E. Iwuoha, A. Nwanya, *Appl. Surf. Sci. Adv.* **2022**, *9*, 100233.
- [17] S. Ullah, P. A. Denis, F. Sato, *Appl. Mater. Today* **2017**, *9*, 333–340.
- [18] C. Sun, D. J. Searles, *J. Phys. Chem. C* **2012**, *116*, 26222–26226.
- [19] M. Wu, Y. Zhao, B. Sun, Z. Sun, C. Li, Y. Han, L. Xu, Z. Ge, Y. Ren, M. Zhang, Q. Zhang, Y. Lu, W. Wang, Y. Ma, Y. Chen, *Nano Energy* **2020**, *70*, 104498.
- [20] a) F. Jiang, Y. Wang, T. Qiu, Y. Zhang, W. Zhu, C. Yang, J. Huang, Z. Fang, G. Dai, *ACS Appl. Mater. Interfaces* **2021**, *13*, 48818–48827; b) B. Ball, C. Chakravarty, P. Sarkar, *J. Phys. Chem. C* **2019**, *50*, 30155–30164.
- [21] a) Z. Yang, J. Tian, Z. Yin, C. Cui, W. Qian, F. Wei, *Carbon* **2019**, *141*, 467–480; b) Y. Liang, W. H. Lai, Z. Miao, S. L. Chou, *Small* **2018**, *14*, 1702514.
- [22] a) G. Li, Y. Li, H. Liu, Y. Guo, Y. Li, D. Zhu, *Chem. Commun.* **2010**, *46*, 3256–3258; b) Y. Fang, Y. Liu, L. Qi, Y. Xue, Y. Li, *Chem. Soc. Rev.* **2022**, *51*, 2681–2709; c) N. N. Pham, *Appl. Surf. Sci. Adv.* **2022**, *11*, 100301.
- [23] Q. Zhang, C. Tang, L. Fu, *Appl. Surf. Sci.* **2019**, *497*, 143723.
- [24] O. V. Kharissova, B. I. Kharisov, *RSC Adv.* **2014**, *4*, 30807–30815.
- [25] a) F. Zhang, E. Alhajji, Y. Lei, N. Kurra, H. N. Alshareef, *Adv. Energy Mater.* **2018**, *8*, 1800353; b) D. Wang, Z. Wang, Y. Li, K. Dong, J. Shao, S. Luo, Y. Liu, X. Qi, *Appl. Surf. Sci.* **2019**, *464*, 422–428; c) Y. Xu, C. Zhang, M. Zhou, Q. Fu, C. Zhao, M. Wu, Y. Lei, *Nat. Commun.* **2018**, *9*, 1720; d) X. Hu, X. Sun, S. J. Yoo, B. Evanko, F. Fan, S. Cai, C. Zheng, W. Hu, G. D. Stucky, *Nano Energy* **2019**, *56*, 828–839.
- [26] Q. Lv, W. Si, Z. Yang, N. Wang, Z. Tu, Y. Yi, C. Huang, L. Jiang, M. Zhang, J. He, *ACS Appl. Mater. Interfaces* **2017**, *9*, 29744–29752.
- [27] a) Q. Lv, W. Si, J. He, L. Sun, C. Zhang, N. Wang, Z. Yang, X. Li, X. Wang, W. Deng, *Nat. Commun.* **2018**, *9*, 1–11; b) Y. Zhao, J. Wan, H. Yao, L. Zhang, K. Lin, L. Wang, N. Yang, D. Liu, L. Song, J. Zhu, *Nature Chem.* **2018**, *10*, 924–931; c) W. Sun, S. X. Dou, *Chem* **2018**, *4*, 2024–2026.
- [28] R. Liu, H. Liu, Y. Li, Y. Yi, X. Shang, S. Zhang, X. Yu, S. Zhang, H. Cao, G. Zhang, *Nanoscale* **2014**, *6*, 11336–11343.
- [29] J. P. Perdew, K. Burke, M. Ernzerhof, *Phys. Rev. Lett.* **1996**, *77*, 3865.
- [30] a) G. Kresse, D. Joubert, *Phys. Rev. B* **1999**, *59*, 1758; b) G. Kresse, J. Furthmüller, *Physical review B* **1996**, *54*, 11169; c) G. Kresse, J. Furthmüller, *Comput. Mater. Sci.* **1996**, *6*, 15–50.
- [31] a) N. N. Pham, S. G. Kang, Y.-A. Son, S. Y. Lee, H.-J. Kim, S. G. Lee, *J. Phys. Chem. C* **2019**, *123*, 27483–27491; b) N. N. Pham, J. S. Park, H.-T. Kim, H.-J. Kim, Y.-A. Son, S. G. Kang, S. G. Lee, *New J. Chem.* **2019**, *43*, 348–355; c) O. L. Li, N. N. Pham, J. Kim, H. Choi, D. H. Lee, Y. Yang, W. Yao, Y.-R. Cho, S. G. Lee, *Appl. Surf. Sci.* **2020**, *528*, 146979; d) H. W. Lee, H. S. Moon, J. Hur, I. T. Kim, M. S. Park, J. M. Yun, K. H. Kim, S. G. Lee, *Carbon* **2017**, *119*, 492–501; e) N. N. Pham, K. H. Kim, B. Han, S. G. Lee, *J. Phys. Chem. C* **2022**, *126*, 5863–5872; f) J. H. Lee, S. H. Kwon, S. Kwon, M. Cho, K. H. Kim, T. H. Han, S. G. Lee, *Nanomaterials* **2019**, *9*, 268.
- [32] S. Grimme, J. Antony, S. Ehrlich, H. Krieg, *J. Chem. Phys.* **2010**, *132*, 154104.
- [33] Q. Zheng, G. Luo, Q. Liu, R. Quhe, J. Zheng, K. Tang, Z. Gao, S. Nagase, J. Lu, *Nanoscale* **2012**, *4*, 3990–3996.
- [34] a) Z. Zheng, Y. Xue, Y. Li, *Trends Chem.* **2022**, *4*, 754–768; b) H. Bao, L. Wang, C. Li, J. Luo, *ACS Appl. Mater. Interfaces* **2018**, *11*, 2717–2729.
- [35] F. Juarez, F. Dominguez-Flores, A. Goduljan, L. Mohammadzadeh, P. Quaino, E. Santos, W. Schmickler, *Carbon* **2018**, *139*, 808–812.
- [36] a) D. Gaissmaier, M. van den Borg, D. Fantauzzi, T. Jacob, *ChemSusChem* **2020**, *13*, 771–783. b) D. Gaissmaier, D. Fantauzzi, T. Jacob, *J. Chem. Phys.* **2019**, *150*, 041723.
- [37] B. Jang, J. Koo, M. Park, H. Lee, J. Nam, Y. Kwon, H. Lee, *Appl. Phys. Lett.* **2013**, *103*, 263904.
- [38] H. Zhang, M. Zhao, X. He, Z. Wang, X. Zhang, X. Liu, *J. Phys. Chem. C* **2011**, *115*, 8845–8850.
- [39] a) Y. Wang, Q. Zhang, M. Jia, D. Yang, J. Wang, M. Li, J. Zhang, Q. Sun, Y. Jia, *Appl. Surf. Sci.* **2016**, *363*, 318–322; b) J. Zhang, G. Liu, H. Hu, L. Wu, Q. Wang, X. Xin, S. Li, P. Lu, *Appl. Surf. Sci.* **2019**, *487*, 1026–1032; c) Y. Shaidi, E. Kucukbenli, S. De Gironcoli, *J. Phys. Chem. C* **2018**, *122*, 20800–20808; d) H. Zhang, Y. Yang, D. Ren, L. Wang, X. He, *Energy Storage Mater.* **2021**, *36*, 147–170; e) R. A. DiLeo, A. Castiglia, M. J. Ganter, R. E. Rogers, C. D. Cress, R. P. Raffaele, B. J. Landi, *Acs Nano* **2010**, *4*, 6121–6131; f) J. Liu, T. Zhao, S. Zhang, Q. Wang, *Nano Energy* **2017**, *38*, 263–270.

Manuscript received: May 30, 2024

Revised manuscript received: August 23, 2024

Accepted manuscript online: September 19, 2024

Version of record online: November 4, 2024